DOI:https://doi.org/10.30742/b51bvx32 e-ISSN 2685-8894; p-ISSN 2460-9773
Jurnal Vitek Bidang Kedokteran Hewan Vol.16 No.1, Mei 2026

IN SILICO EVALUATION OF *Physalis angulata* SECONDARY METABOLITES AS POTENTIAL QcrB INHIBITORS IN *Mycobacterium tuberculosis* AND *Mycobacterium bovis*

Zahir Thoriq[1*], Lia Puspitasari[2], Lita Rakhma Yustinasari[3], Suryo Kuncorojakti[4], Tarshan Sharma Suresh[5]

[1*] Master's Program in Vaccinology and Immunotherapeutics, Faculty of Veterinary Medicine, Universitas Airlangga, Surabaya, Indonesia
email: zahir.thoriq-2024@fkh.unair.ac.id

[2] Department of Pharmacy, Faculty of Mathematics and Natural Sciences, Universitas Sebelas Maret, Indonesia
email: lia.puspitasari@staff.uns.ac.id

[3] Department of Veterinary Science, Faculty of Veterinary Medicine, Universitas Airlangga, Surabaya, Indonesia
email: lita-r-y@fkh.unair.ac.id

[4] Department of Veterinary Science, Faculty of Veterinary Medicine, Universitas Airlangga, Surabaya, Indonesia
email: suryokuncorojakti@fkh.unair.ac.id

[5] Master's Program in Reproductive Biology, Faculty of Veterinary Medicine, Universitas Airlangga, Surabaya, Indonesia
email: tarshan40@gmail.com

Received : 03 March 2026
Accepted : 03 March 2026
Published : 25 Mei 2026

Abstract

Antimicrobial resistance in Mycobacterium tuberculosis and Mycobacterium bovis remains a major concern in both human and veterinary health, underscoring the urgent need for novel therapeutic targets and bioactive compounds. This study aimed to assess the potential of secondary metabolites from Physalis angulata as QcrB inhibitors using an in silico approach. Alignment of QcrB amino acid sequences from both species showed 100% sequence identity, suggesting that compounds capable of engaging the QcrB active site in M. tuberculosis would be expected to show a similar binding profile in M. bovis. From 51 identified metabolites, nine fulfilled drug-likeness and safety criteria and were advanced to docking evaluation. Docking simulations showed that four metabolites successfully occupied the QcrB binding pocket, with withaphysanolide A showing the most promising interaction profile through engagement with six key residues associated with QcrB inhibition. ADMET predictions indicated that withaphysanolide A possesses advantageous characteristics, including high intestinal absorption, absence of CYP450 inhibition, and lack of major toxicity alerts. These findings suggest that withaphysanolide A is a promising candidate for further investigation as a potential QcrB-targeting antimycobacterial compound, warranting validation through in vitro and in vivo studies.

Keywords: *in silico, Mycobacterium bovis, Mycobacterium tuberculosis, Physalis angulata, QcrB*

INTRODUCTION

The *Mycobacterium tuberculosis* complex (MTBC) constitutes a group of phylogenetically closely related bacteria responsible for tuberculosis. Members of the complex are classified into human-adapted and animal-adapted lineages, with *Mycobacterium bovis*, which predominantly infects cattle, representing one of the principal animal adapted variants. Several strains within the

human-adapted lineages exhibit anthroponotic transmission, whereas certain animal-adapted strains are capable of zoonotic transmission, thereby contributing to broader public health risks (Hubálek, 2003; Silva et al., 2022).

One of the major challenges in addressing infections caused by *Mycobacterium* species is the widespread phenomenon of antimicrobial resistance. In humans, drug-resistant tuberculosis encompasses several levels of resistance, each carrying distinct epidemiological burdens. The most common form, and the primary indicator used by the World Health Organization (WHO), is rifampicin-resistant tuberculosis (RR-TB). In 2024, an estimated 390,000 RR-TB cases were reported globally; however, only 164,545 individuals (42%) were able to access treatment, highlighting a substantial gap in therapeutic coverage. Because rifampicin resistance is strongly correlated with isoniazid resistance, RR-TB figures are also used operationally to approximate the burden of multidrug-resistant tuberculosis (MDR-TB). Consequently, the global prevalence of MDR-TB is estimated to be similar to that of RR-TB. A more severe form of resistance, extensively drug-resistant tuberculosis (XDR-TB), is defined as MDR-TB accompanied by additional resistance to fluoroquinolones and at least one second-line agent. Although its prevalence is lower than that of MDR-TB, XDR-TB poses the most critical clinical threat due to its low treatment success rates and the limited therapeutic options available (World Health Organization, 2025).

A comparable situation is also observed in *M. bovis*. Abdelsadek et al. (2020) reported that susceptibility testing of isolates obtained from raw milk, lymph nodes, and sputum of cattle revealed very high resistance rates to pyrazinamide (78.5%) and isoniazid (59.3%), followed by moderate resistance to rifampicin (40.7%) and ethambutol (31.8%). Additionally, resistance to second-line agents, particularly kanamycin (82.3%) and amikacin (80.7%), further highlights the growing risk associated with multidrug-resistant *M. bovis* strains.

Various strategies have been explored to address the growing challenge of antimicrobial resistance, including the identification of novel therapeutic targets and the discovery of new compounds capable of disrupting essential biological processes in *M. tuberculosis* and related species. One protein that has emerged as a particularly promising target is QcrB, a key subunit of the cytochrome bc_1 complex. QcrB plays a central role in coordinating the function of the cytochrome bc_1 complex within the respiratory electron transport chain (ETC) of *Mycobacterium* (Bahuguna et al., 2021; Ko & Choi, 2016). Inhibition of QcrB collapses the proton motive force and impairs ATP synthesis, leading to rapid bactericidal activity against both replicating and dormant mycobacterial populations (Imran et al., 2023). Owing to this essential role, QcrB continues to attract interest as a validated and highly specific drug target.

In the search for potential QcrB inhibitors, secondary metabolites from *Physalis angulata* represent a promising source of bioactive compounds. This premise is supported by the findings of Pietro et al. (2000), who reported that extracts of *P. angulata* exhibit notable antimicrobial activity against several *Mycobacterium* species, including *M. tuberculosis*, *M. kansasii*, *M. avium*, *M. malmoense*, and *M. intracellulare*. These observations suggest that *P. angulata* possesses a broad spectrum of antimyobacterial activity, making its secondary metabolites attractive candidates for further investigation against QcrB.

Building on this evidence, the present study aims to evaluate, through an in silico approach, the potential of secondary metabolites from *P. angulata* as inhibitors targeting the QcrB protein of *M. tuberculosis* and *M. bovis*. This evaluation includes sequence analysis of QcrB, molecular docking, interaction profiling, and ADMET prediction to identify promising lead compounds for subsequent empirical validation. To the best of our knowledge, this study provides the first in silico evaluation of secondary metabolites from *P. angulata* against the QcrB protein of both *M. tuberculosis* and *M. bovis*, offering preliminary molecular insights into their inhibitory potential.

MATERIALS AND METHODS

Protein and Ligand Data Retrieval

Amino acid sequences of QcrB from *M. tuberculosis* (UniProt ID: P9WP37) and *M. bovis* (UniProt ID: P63886) were obtained from

the UniProt database. The three-dimensional (3D) structural model of *M. tuberculosis* QcrB was retrieved from the AlphaFold Protein Structure Database. Telacebec was selected as the reference ligand for docking validation, whereas secondary metabolites of *P. angulata* were compiled based on previously published reports (Zhou et al., 2021). All ligand structures used in this study were downloaded from the PubChem database.

Global Alignment of Protein Sequences

Amino acid sequences of QcrB from *M. tuberculosis* and *M. bovis* were aligned using the Clustal Omega web server, with the sequences formatted in FASTA.

Secondary Metabolite Screening

Ligand screening was carried out to identify compounds that fulfilled the established selection parameters. Molecular property assessment and toxicity prediction were conducted using DataWarrior V6.1.0 and pkCSM.

The screening criteria were based primarily on Lipinski's Rule of Five, which states that orally active drug-like molecules generally exhibit a molecular mass ≤ 500 Da, ≤ 10 hydrogen bond acceptors, ≤ 5 hydrogen bond donors, lipophilicity within $-2 \leq \text{clogP} \leq 5$, and ≤ 5 rotatable bonds (Barret, 2018). Compounds failing at least two of these parameters are more likely to present absorption, distribution, metabolism, excretion, and toxicity (ADMET)-related limitations. Additional filters required a polar surface area ≤ 140 Å² and the exclusion of compounds predicted to exhibit any of the following: human ether-à-go-go related gene I and II (hERG I and II) inhibition, hepatotoxicity, mutagenic, tumorigenic, irritant, and reproductive toxicities (Veber et al., 2002).

Key Residues in the QcrB Protein Binding Site

The binding pocket used in this study was defined based on the amino acid residues reported to interact with the reference ligand telacebec in the work of Zhou et al. (2021). Their analysis identified twelve QcrB residues involved in ligand binding: Tyr164, Gly175, Ala179, Leu180, Thr184, Ser304, Pro306, Met310, Thr313, Glu314, Ala317, and Met342.

Pre-Molecular Docking Preparation

Protein and ligand preparation was performed using MOE v2014.09. For protein preparation, undesired chains, residues, and molecular groups were removed prior to optimization. The Amber10: EHT force field was applied, and calculations were conducted under gas-phase solvation. Protonation and energy minimization were carried out to restore missing hydrogen atoms and obtain the lowest-energy conformation, using an energy gradient of 0.05 RMS kcal/mol·Å (Ekawati et al., 2019). Partial charge calculation was also included in this stage (Nasution et al., 2017).

Ligand preparation was conducted through the MOE Database Viewer, beginning with the Wash function. The MMFF94x force field was used, and energy minimization was performed until reaching a gradient threshold of 0.001 RMS kcal/mol·Å (Ekawati et al., 2019).

Molecular Docking Simulation

Molecular docking was performed using MOE v2014.09 with a flexible docking approach. The "Induced Fit" protocol was applied, employing the Triangle Matcher placement method with London dG scoring and a retain value of 50. Refinement was conducted using the force field method, followed by GBVI/WSA dG rescoring, with the final retain value set to 1 (Nasution et al., 2017).

Protein–Ligand Interaction Visualization

Protein–ligand interaction visualization was carried out using MOE v2014.09. The interaction analyses were generated based on the results obtained from the molecular docking simulation.

Prediction of Ligand ADMET Characteristics

ADMET characteristics of the ligands were predicted using DataWarrior, pkCSM, and SwissADME. Predictions generated using pkCSM and SwissADME required simplified molecular-input line-entry system (SMILES) strings as input, which were obtained from the PubChem database.

RESULTS

Protein and Ligand Data Overview

The QcrB protein sequence of *M. tuberculosis* used in this study was obtained from strain ATCC 25618/H37Rv, whereas the QcrB sequence of *M. bovis* originated from strain ATCC BAA-935/AF2122. Both sequences comprise 549 amino acids, and the global alignment analysis showed 100% identity between them, as presented in Figure 1. Given this complete sequence conservation, the subsequent molecular docking simulations could therefore be conducted using the 3D protein structure from either species.

Based on literature screening, a total of 51 secondary metabolites of *P. angulata* were identified (Ayodhyareddy & Rupa, 2013; Hoang et al., 2018; Rengifo-Salgado & Vargas-Arana, 2013). The metabolites, along with the reference ligand, are summarized in Table 1.

Secondary Metabolite Screening Results

A total of nine out of the 51 identified secondary metabolites passed the screening criteria and were subsequently selected for molecular docking simulations. These compounds were withangulatin A, physalin B, withaminimin, withangulatin I, physalin J, physalin F, physagulin A, withaphysanolide A, and physanolide A.

Molecular Docking and Protein–Ligand Interaction Results

Of the nine secondary metabolites evaluated as test ligands, only four successfully docked into the QcrB binding pocket. These ligands were withangulatin A, withangulatin I, physagulin A, and withaphysanolide A.

The reference ligand telacebec exhibited the most favorable binding free energy ($\Delta G_{binding}$) among all compounds evaluated (Table 2). Analysis of the protein–ligand interaction profile showed that telacebec interacted with 19 amino acid residues within the QcrB binding pocket, nine of which correspond to the key residues previously reported in the literature (Figure 3). The interaction visualization further demonstrated that multiple ligand atoms contributed to contacts with pocket residues. Although the specific interaction types are not explicitly labeled in the diagram, examination of the atomic contacts and symbols indicates a combination of polar and non-polar interactions forming the overall binding network.

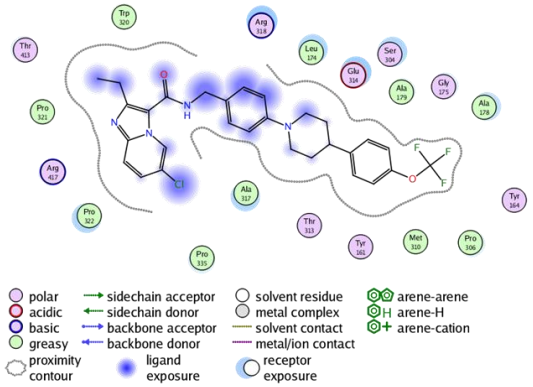

Figure 2. Interaction Map of Telacebec within the QcrB Binding Pocket

Among the four secondary metabolites that successfully docked within the QcrB binding site, withaphysanolide A demonstrated the most favorable profile as a potential QcrB inhibitor. Although its binding free energy was not lower than that of physagulin A, withaphysanolide A interacted with a greater number of the reference key residues. In addition, the interaction pattern observed within the binding pocket indicates a combination of polar and non-polar interactions (Figure 3).

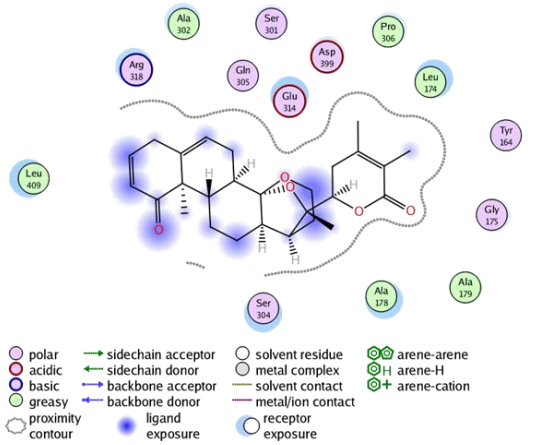

Figure 3. Interaction Map of Withaphysanolide A within the QcrB Binding Pocket

Predicted ADMET Profiles

Comparison of the ADMET profiles of telacebec and withaphysanolide A shows that each compound demonstrates advantages across different ADMET parameters. Withaphysanolide A is predicted to show favorable values in parameters such as intestinal absorption, volume of distribution at steady state (VDss), fraction unbound, the absence of inhibitory activity toward any

cytochrome P450 (CYP450) isoforms, and the lack of toxicity-related alerts. In contrast, telacebec performs better in parameters including aqueous solubility, blood–brain barrier (BBB) and central nervous system (CNS) permeability, and maximum tolerated dose. The complete ADMET profiles for both compounds are presented in Table 3.

DISCUSSION

The 100% sequence identity observed between QcrB from *M. tuberculosis* and *M. bovis* indicates that QcrB is a highly suitable inhibitory target for therapeutic strategies aimed at both species. This full conservation suggests that the 3D architecture of the protein, including the configuration of the binding pocket and the arrangement of key interacting residues, is essentially identical in the two organisms. Consequently, inhibitors designed to bind QcrB of *M. tuberculosis* are expected to exhibit comparable binding affinity and interaction patterns toward QcrB of *M. bovis*, supporting the feasibility of a unified inhibition approach for both pathogens.

Telacebec was employed as the reference ligand because it represents a next-generation imidazopyridine amide antituberculosis candidate specifically developed to inhibit QcrB and has advanced through phase I and II clinical trials (Imran et al., 2023). Validation of the molecular docking simulation showed that telacebec exhibited the strongest binding affinity toward QcrB compared with the tested metabolites. However, it interacted with only nine of the 12 predefined reference key residues. This indicates that the docked conformation obtained in silico may differ from the interaction pattern observed experimentally. The structural model generated by the AlphaFold Protein Structure Database likely presents a binding pocket configuration that deviates from the QcrB–telacebec complex resolved via Cryo-EM as reported by Zhou et al. (2021). The reference residues used in this study were derived from that experimental Cryo-EM structure, in which QcrB was inhibited by telacebec. These structural discrepancies may account for the difference in telacebec's binding pose, particularly because the docking simulations were performed using a rigid protein backbone, whereas the biological binding pocket exhibits inherent conformational flexibility (Stank et al., 2016).

The molecular docking simulations indicate that withaphysanolide A, a secondary metabolite of *P. angulata*, shows the greatest potential as a QcrB inhibitor among the metabolites analyzed. Although its binding free energy was slightly less negative than that of physagulin A, which reflects a comparatively weaker interaction within the QcrB binding pocket, withaphysanolide A displayed the highest number of matching interactions with the reference key residues, totaling six residues (Du et al., 2016). This correspondence with the reference residues is important because it suggests that the ligand engages amino acids involved in the normal biological function of QcrB, indicating a possible occupation of functionally relevant regions within the pocket (Sliwoski et al., 2014). When compared with the reference ligand telacebec, the binding free energy of withaphysanolide A was less negative, which is expected given the molecular size difference. The larger structure of telacebec provides more opportunities for contact with binding pocket residues, contributing to its stronger predicted binding affinity relative to withaphysanolide A.

The ADMET predictions collectively indicate that withaphysanolide A possesses several advantages relative to telacebec. In the absorption category, withaphysanolide A shows a higher predicted intestinal absorption percentage, suggesting greater oral bioavailability potential even though both compounds may be affected by P glycoprotein–mediated efflux (Mora Lagares et al., 2022). In the distribution category, withaphysanolide A demonstrates a higher predicted steady state volume of distribution and a greater fraction unbound in plasma, indicating improved systemic availability compared with telacebec (Pires et al., 2015). In the metabolism category, withaphysanolide A displays a more favorable enzymatic profile, as it is predicted to be a substrate of CYP3A4 but not an inhibitor of other CYP450 isoforms, suggesting a lower likelihood of drug–drug interactions and a safer metabolic pathway than telacebec (Abdelmonem et al., 2024; Zhang et al., 2024). In the excretion category, withaphysanolide A exhibits a lower predicted total clearance, implying slower elimination and the potential

for prolonged systemic exposure. Finally, in the toxicity category, withaphysanolide A shows a more favorable profile because it is not predicted to inhibit the hERG II channel nor exhibit hepatotoxic potential, although it presents a lower maximum tolerated dose than telacebec. Collectively, these findings support the interpretation that withaphysanolide A possesses comparatively advantageous ADMET characteristics that strengthen its potential as a promising QcrB inhibitor candidate.

The findings obtained in this study provide an initial indication that withaphysanolide A, a secondary metabolite of *P. angulata*, has potential as an inhibitor of the QcrB protein from *M. tuberculosis* and *M. bovis*. . Nonetheless, several limitations must be considered, including the use of a rigid binding pocket during docking simulations and the fact that many of the predictive parameters and computational models employed were developed primarily for human biological systems rather than for non-human species such as cattle. Consequently, these predictions require confirmation through in vitro and in vivo experimentation, as in silico outcomes are inherently probabilistic and may not fully capture biological behavior. The importance of such validation is underscored by the findings of Malík et al. (2021), who demonstrated that telacebec did not inhibit hERG channels or CYP450 isoenzymes in in vitro assays, despite contrary predictions generated by computational models. Therefore, empirical studies are essential to substantiate the inhibitory potential of withaphysanolide A and to assess its suitability for further development as a therapeutic candidate targeting QcrB in *M. tuberculosis* and *M. bovis*.

CONCLUSION

In silico evaluation demonstrated that the QcrB proteins of *M. tuberculosis* and *M. bovis* share 100% sequence identity, indicating that inhibitors designed to target the QcrB of *M. tuberculosis* are expected to exhibit comparable binding affinity and interaction patterns toward the QcrB of *M. bovis*. Among the secondary metabolites of *P. angulata*, withaphysanolide A emerged as the best overall candidate, supported by its binding free energy (−5.5532 kcal/mol) and its interactions with six of the 12 reference key residues within the QcrB binding pocket. ADMET predictions further indicated that this compound possesses a favorable safety profile for therapeutic use. Nonetheless, empirical data derived from in vitro and in vivo studies remain necessary to validate its inhibitory activity and confirm its suitability as a therapeutic candidate against *M. tuberculosis* and *M. bovis* infections.

REFERENCE

Abdelmonem, B. H., Abdelaal, N. M., Anwer, E. K. E., Rashwan, A. A., Hussein, M. A., Ahmed, Y. F., Khashana, R., Hanna, M. M., & Abdelnaser, A. (2024). Decoding the role of CYP450 enzymes in metabolism and disease: A comprehensive review. *Biomedicines*, 12(7), 1467. https://doi.org/10.3390/biomedicines12071467

Abdelsadek, H. A., Sobhy, H. M., Mohamed, K. F., Hekal, S. H. A., Dapgh, A. N., & Hakim, A. S. (2020). Multidrug-resistant strains of *Mycobacterium* complex species in Egyptian farm animals, veterinarians, and farm and abattoir workers. *Veterinary World*, 13(10), 2150–2155. https://doi.org/10.14202/vetworld.2020.2150-2155

Ayodhyareddy, P., & Rupa, P. (2016). Ethno medicinal, phyto chemical and therapeutic importance of *Physalis angulata* L.: A review. *International Journal of Science and Research*, 5(5), 2122–2127.

Bahuguna, A., Rawat, S., & Rawat, D. S. (2021). QcrB in *Mycobacterium tuberculosis*: The new drug target of antitubercular agents. *Medicinal Research Reviews*, 41(4), 2565–2581. https://doi.org/10.1002/med.21779

Barret, R. (2018). 6 – Lipinski's rule of five. In *Therapeutical chemistry: Fundamentals* (pp. 97–100). Elsevier. https://doi.org/10.1016/B978-1-78548-288-5.50006-8

Du, X., Li, Y., Xia, Y.-L., Ai, S.-M., Liang, J., Sang, P., Ji, X.-L., & Liu, S.-Q. (2016). Insights into protein–ligand interactions: Mechanisms, models, and methods. *International Journal of Molecular*

Sciences, 17(1), 144. https://doi.org/10.3390/ijms17020144

Ekawati, M. M., Nasution, M. A. F., Siregar, S., Rizki, I. F., & Tambunan, U. S. F. (2019). Pharmacophore-based virtual screening and molecular docking simulation of terpenoid compounds as the inhibitor of sonic hedgehog protein for colorectal cancer therapy. *IOP Conference Series: Materials Science and Engineering*, 509, 012075. https://doi.org/10.1088/1757-899X/509/1/012075

Hoang, L. T. A., Do, T. T., Duong, T. D., Phan, V. K., Tran, H. Q., Pham, T. H. Y., Do, T. T., Pham, V. C., Le, C. V. C., & Tran, M. H. (2018). Phytochemical constituents and cytotoxic activity of *Physalis angulata* L. growing in Vietnam. *Phytochemistry Letters*, 27, 193–196. https://doi.org/10.1016/j.phytol.2018.07.029

Hubálek, Z. (2003). Emerging human infectious diseases: Anthropo-noses, zoonoses, and sapronoses. *Emerging Infectious Diseases*, 9(3), 403–404. https://doi.org/10.3201/eid0903.020208

Imran, M., Abida, A., Alotaibi, N. M., Thabet, H. K., Alruwaili, J. A., Asdaq, S. M. B., Eltaib, L., Alshehri, A., Alsaiari, A. A., Almehmadi, M., Alshammari, A. B. H., & Alshammari, A. M. (2023). QcrB inhibition as a potential approach for the treatment of tuberculosis: A review of recent developments, patents, and future directions. *Journal of Infection and Public Health*, 16(7), 928–937. https://doi.org/10.1016/j.jiph.2023.04.011

Ko, Y., & Choi, I. (2016). Putative 3D structure of QcrB from *Mycobacterium tuberculosis* cytochrome bc_1 complex, a novel drug-target for new series of antituberculosis agent Q203. *Bulletin of the Korean Chemical Society*, 37(5), 725–731. https://doi.org/10.1002/bkcs.10765

Malík, I., Čižmárik, J., Kováč, G., Pecháčová, M., & Hudecová, L. (2021). Telacebec (Q203): Is there a novel effective and safe anti-tuberculosis drug on the horizon? *Česká a slovenská farmacie*, 70, 164–171.

Mora Lagares, L., Pérez-Castillo, Y., Minovski, N., & Novi č, M. (2022). Structure–function relationships in the human P-glycoprotein (ABCB1): Insights from molecular dynamics simulations. *International Journal of Molecular Sciences*, 23(1), 362. https://doi.org/10.3390/ijms23010362

Nasution, M. A. F., Aini, R. N., & Tambunan, U. S. F. (2017). Virtual screening of commercial cyclic peptides as NS2B-NS3 protease inhibitor of dengue virus serotype 2 through molecular docking simulation. *IOP Conference Series: Materials Science and Engineering*, 188, 012017. https://doi.org/10.1088/1757-899X/188/1/012017

Pietro, R. C. L. R., Kashima, S., Sato, D. N., Januário, A. H., & França, S. C. (2000). In vitro antimycobacterial activities of *Physalis angulata* L. *Phytomedicine*, 7(4), 335–338.

Pires, D. E. V., Blundell, T. L., & Ascher, D. B. (2015). pkCSM: Predicting small-molecule pharmacokinetic and toxicity properties using graph-based signatures. *Journal of Medicinal Chemistry*, 58(9), 4066–4072. https://doi.org/10.1021/acs.jmedchem.5b00104

Rengifo-Salgado, E., & Vargas-Arana, G. (2013). *Physalis angulata* L. (Bolsa Mullaca): A review of its traditional uses, chemistry and pharmacology. *Boletín Latinoamericano y del Caribe de Plantas Medicinales y Aromáticas*, 12(5), 431–445.

Silva, M. L., Cá, B., Osório, N. S., Rodrigues, P. N. S., Maceiras, A. R., & Saraiva, M. (2022). Tuberculosis caused by *Mycobacterium africanum*: Knowns and unknowns. *PLOS Pathogens*, 18(5), e1010490. https://doi.org/10.1371/journal.ppat.1010490

Sliwoski, G., Kothiwale, S., Meiler, J., & Lowe, E. W., Jr. (2014). Computational methods in drug discovery. *Pharmacological Reviews*, 66(1), 334–395. https://doi.org/10.1124/pr.112.007336

Stank, A., Kokh, D. B., Fuller, J. C., & Wade, R. C. (2016). Protein binding pocket dynamics. *Accounts of Chemical Research*, 49(4), 809–815.

https://doi.org/10.1021/acs.accounts.5b00516

Veber, D. F., Johnson, S. R., Cheng, H. Y., Smith, B. R., Ward, K. W., & Kopple, K. D. (2002). Molecular properties that influence the oral bioavailability of drug candidates. *Journal of Medicinal Chemistry*, 45(12), 2615–2623. https://doi.org/10.1021/jm020017n

World Health Organization. (2025). *Global tuberculosis report 2025*. World Health Organization.

Zhang, Y., Wang, Z., Wang, Y., Jin, W., Zhang, Z., Jin, L., Qian, J., & Zheng, L. (2024). CYP3A4 and CYP3A5: The crucial roles in clinical drug metabolism and the significant implications of genetic polymorphisms. *PeerJ*, 12, e18636. https://doi.org/10.7717/peerj.18636

Zhou, S., Wang, W., Zhou, X., Zhang, Y., Lai, Y., Tang, Y., Xu, J., Li, D., Lin, J., Yang, X., Ran, T., Chen, H., Guddat, L. W., Wang, Q., Gao, Y., Rao, Z., & Gong, H. (2021). Structure of *Mycobacterium tuberculosis* cytochrome bcc in complex with Q203 and TB47, two anti-TB drug candidates. *eLife*, 10, e69418. https://doi.org/10.7554/eLife.69418

```
P9WP37      MSPKLSPPNIGEVLARQAEDIDTRYHPSAALRRQLNKVFPTHWSFLLGEIALYSFVVLLI      60
P63886      MSPKLSPPNIGEVLARQAEDIDTRYHPSAALRRQLNKVFPTHWSFLLGEIALYSFVVLLI      60
            ************************************************************

P9WP37      TGVYLTLFFDPSMVDVTYNGVYQPLRGVEMSRAYQSALDISFEVRGGLFVRQIHHWAALM      120
P63886      TGVYLTLFFDPSMVDVTYNGVYQPLRGVEMSRAYQSALDISFEVRGGLFVRQIHHWAALM      120
            ************************************************************

P9WP37      FAAAIMVHLARIFFTGAFRRPRETNWVIGSLLLILAMFEGYFGYSLPDDLLSGLGLRAAL      180
P63886      FAAAIMVHLARIFFTGAFRRPRETNWVIGSLLLILAMFEGYFGYSLPDDLLSGLGLRAAL      180
            ************************************************************

P9WP37      SSITLGMPVIGTWLHWALFGGDFPGTILIPRLYALHILLLPGIILALIGLHLALVWFQKH      240
P63886      SSITLGMPVIGTWLHWALFGGDFPGTILIPRLYALHILLLPGIILALIGLHLALVWFQKH      240
            ************************************************************

P9WP37      TQFPGPGRTEHNVVGVRVMPVFAFKSGAFFAAIVGVLGLMGGLLQINPIWNLGPYKPSQV      300
P63886      TQFPGPGRTEHNVVGVRVMPVFAFKSGAFFAAIVGVLGLMGGLLQINPIWNLGPYKPSQV      300
            ************************************************************

P9WP37      SAGSQPDFYMMWTEGLARIWPPWEFYFWHHTIPAPVWVAVIMGLVFVLLPAYPFLEKRFT      360
P63886      SAGSQPDFYMMWTEGLARIWPPWEFYFWHHTIPAPVWVAVIMGLVFVLLPAYPFLEKRFT      360
            ************************************************************

P9WP37      GDYAHHNLLQRPRDVPVRTAIGAMAIAFYMVLTLAAMNDIIALKFHISLNATTWIGRIGM      420
P63886      GDYAHHNLLQRPRDVPVRTAIGAMAIAFYMVLTLAAMNDIIALKFHISLNATTWIGRIGM      420
            ************************************************************

P9WP37      VILPPFVYFITYRWCIGLQRSDRSVLEHGVETGIIKRLPHGAYIELHQPLGPVDEHGHPI      480
P63886      VILPPFVYFITYRWCIGLQRSDRSVLEHGVETGIIKRLPHGAYIELHQPLGPVDEHGHPI      480
            ************************************************************

P9WP37      PLQYQGAPLPKRMNKLGSAGSPGSGSFLFADSAAEDAALREAGHAAEQRALAALREHQDS      540
P63886      PLQYQGAPLPKRMNKLGSAGSPGSGSFLFADSAAEDAALREAGHAAEQRALAALREHQDS      540
            ************************************************************

P9WP37      IMGSPDGEH   549
P63886      IMGSPDGEH   549
            *********
```

Figure 1. Alignment of QcrB Amino Acid Sequences from *M. tuberculosis* (P9WP37) and *M. bovis* (P63886)

Table 1. Dataset of the Reference Ligand Telacebec and Secondary Metabolites of *P. angulata*

CID	Compound Name	CID	Compound Name
68234908	Telacebec	14605184	Ixocarpanolide
305	Choline	16082070	Physagulin L
3220	Emodin	16757497	Withangulatin B
10494	Oleanolic acid	23597327	Physalin C
64945	Ursolic acid	24814495	Withangulatin I
147647	Withangulatin A	42610742	Physagulin J
161671	Withanolide D	44426449	Physalin J
173183	Campesterol	44426450	Physalin U
222284	β-sitosterol	44577487	Physalin A
259846	Lupeol	49864133	Physalin F
265237	Withaferin A	56683730	Physalin G
431000	Physalin B	73816389	Physalin K
431071	Physalin D	74820162	Physagulin F
1794427	Chlorogenic acid	85083174	Physagulin B
5280343	Quercetin	85110396	Physagulin A
5280489	β-carotene	85155112	Physagulin C
5280682	Ayanin	85470089	Physagulin K
5281672	Myricetin	101273380	Physagulin I
10009993	Physagulin E	101273381	Physagulin H
10100412	Physagulin D	101586382	Physalin H
10265686	Phygrine	102153900	Withaphysanolide A
13939886	Vamonolide	102254401	Physanolide A
13962952	Physalin E	102257049	Physagulin M
14216306	Withaminimin	102257050	Physagulin N
14236711	Withanolide B	131751562	Physalin I
14605176	Physangulide	131752708	Physagulin G

Table 2. Binding Energies and Interacting Residues of Docked Ligands

Compound Name	$\Delta G_{binding}$ (kcal/mol)	Interacting Residues
Telacebec	-6.4235	Tyr161, Tyr164, Leu174, Gly175, Ala178, Ala179, Ser304, Pro306, Met310, Thr313, Glu314, Ala317, Arg318, Trp320, Pro321, Pro322, Pro335, Thr413, Arg 417
Withangulatin A	-5.4086	Phe158, Ile183, Thr184, Met187, Leu198, Ala339, Val340, Gly343, Phe346, Val347
Withangulatin I	-4.8070	Phe158, Phe162, Ile183, Thr184, Met187, Leu194, Leu198, Leu215, Leu219, Leu220, Ala339, Val340, Met342, Gly343
Physagulin A	-6.1355	Phe158, Phe162, Leu180, Ile183, Thr184, Leu194, Leu198, Arg211, Leu212, Leu215, Ala339
Withaphysanolide A	-5.5532	Tyr164, Leu174, Gly175, Ala178, Ala179, Ser301, Ala302, Ser304, Gln305, Pro306, Glu314, Arg318, Asp399, Leu409

Table 3. Comparative ADMET Profiles of Telacebec and Withaphysanolide A

Categories	Parameters	Compound Name	
		Telacebec	**Withaphysanolide A**
Absorption	Water solubility (log mol/L)	-3.024	-5.415
	Intestinal absorption (%) (human)	89.425	99.844
	Skin permeability (log Kp)	-2.735	-3.596
	P-glycoprotein substrate	Yes	Yes
	P-glycoprotein I inhibitor	Yes	Yes
	P-glycoprotein II inhibitor	Yes	Yes
Distribution	VDss (human) (log L/kg)	0.356	0.363
	Fraction unbound (human) (Fu)	0.048	0.082
	BBB permeability (log BB)	0.345	-0.197
	CNS permeability (log PS)	-1.577	-2.791
Metabolism	CYP450 substrate	Yes (CYP3A4)	Yes (CYP3A4)
	CYP450 inhibitor	Yes (CYP2C19, CYP2C9, CYP2D6, CYP3A4)	No
Excretion	Total clerance (log ml/min/kg)	0.453	0.376
	Renal OCT2 substrate	Yes	Yes
Toxicity	hERG I inhibitor	No	No
	hERG II inhibitor	Yes	No
	Hepatotoxicity	Yes	No
	Mutagenic	No	No
	Tumorigenic	No	No
	Irritant	No	No
	Reproductive effect	No	No
	Max. tolerated dose (human) (log mg/kg/day)	0.432	-0.703
	Oral rat acute toxicity (LD_{50}) (mol/kg)	2.936	2.034
	Synthetic accessibility	3.57	6.62